CRYSTAL GROWTH & DESIGN

Article

The influence of the amide groups in the CO/N selectivity of a series of isoreticular, interpenetrated metal-organic frameworks

Vahid Safarifard, Sabina Rodríguez-Hermida, Vincent Guillerm, Inhar Imaz, Mina Bigdeli, Alireza A. Tehrani, Jordi Juanhuix, Ali Morsali, Mirian E. Casco, Joaquin Silvestre-Albero, Enrique V Ramos-Fernandez, and Daniel Maspoch

Cryst. Growth Des., **Just Accepted Manuscript** • DOI: 10.1021/acs.cgd.6b01054 • Publication Date (Web): 06 Sep 2016

ACS Publications

Crystal Growth & Design is published by the American Chemical Society. 1155 Sixteenth Street N.W., Washington, DC 20036

The influence of the amide groups in the CO_2/N_2 selectivity of a series of isoreticular, interpenetrated metal-organic frameworks

Vahid Safarifard,[†,‡] Sabina Rodríguez-Hermida,[†] Vincent Guillerm,[†] Inhar Imaz,[†] Mina Bigdeli,[‡] Alireza A. Tehrani,[‡] Jordi Juanhuix,[§] Ali Morsali,[‡*] Mirian E. Casco,[⊥] Joaquín Silvestre-Albero,[⊥] Enrique V. Ramos-Fernandez[⊥] and Daniel Maspoch[†,#*]

[†] Catalan Institute of Nanoscience and Nanotechnology (ICN2), CSIC and The Barcelona Institute of Science and Technology, Campus UAB, Bellaterra, 08193 Barcelona, Spain. [‡] Department of Chemistry, Faculty of Sciences, Tarbiat Modares University, P.O. Box 14115-175, Tehran, Islamic Republic of Iran. [§] ALBA Synchrotron, 08290 Cerdanyola del Vallès, Barcelona, Spain. [⊥] Laboratorio de Materiales Avanzados, Departamento de Química Inorgánica-Instituto Universitario de Materiales, Universidad de Alicante, Ctra. San Vicente-Alicante s/n, 03690 San Vicente de Raspeig, Spain. [#] ICREA, Pg. Lluís Companys 23, 08010 Barcelona, Spain.

Metal-Organic Frameworks, Amide, Adsorption, Separation, Breakthrough

ABSTRACT: Here we report the use of a pillaring strategy for the design and synthesis of three novel amide-functionalized metal-organic frameworks (MOFs), **TMUs-22/-23/-24**, isoreticular to the recently reported imine-functionalized **TMU-6** and **TMU-21** MOFs. An extensive study of their CO_2 sorption properties and selectivity for CO_2 over N_2, from single gas sorption isotherms to breakthrough measurements, revealed that not only the incorporation of amide groups but also their accessibility is crucial to obtain enhanced CO_2 sorption and CO_2/N_2 selectivity. Therefore, the MOF with more accessible amide groups (**TMU-24**) shows a CO_2/N_2 selectivity value of ca. 10 (as revealed by breakthrough experiments), which is ca. 500 % and 700 % of the selectivity values observed for the other amide-containing (**TMU-22** and **TMU-23**) and imine-containing (**TMU-6** and **TMU-21**) MOFs.

INTRODUCTION

Microporous metal−organic frameworks (MOFs), constructed from metal-based nodes and polytopic organic ligands, are a promising class of porous materials for carbon capture, separation and storage owing to their very high surface areas, tuneable pore sizes and shapes, and adjustable pore surface functionality.[1-3] For these specific applications, it is widely accepted that certain chemical functionalities located at the pore surfaces of MOFs can increase their CO_2 uptake and selectivity.[4-10] Among these functionalities, CO_2 has been found to bind at unsaturated metal centres *via* the electron rich terminal oxygen atom[11-13]. Also, CO_2 can interact with electron rich Lewis basic groups *via* electron deficient carbon atom.[14] For this purpose, most efforts have been made on the direct and post-synthetic functionalization of MOFs with amine groups.[15-18] More recently, another approach based on the combined optimization of pore size and high charge density has anticipated very promising results.[4, 19, 20]

Besides the use of amine groups, the intrinsic characteristics of the amide groups make them also very attractive to establish cooperative intermolecular interactions with CO_2.[21] Amide groups possess two types of donor-acceptor affinity sites: the -NH moiety that can act as an electron acceptor (Lewis acid), and the -C=O group that can act as an electron donor (Lewis base); both allowing to establish NH···OCO and NC=O···CO_2 interactions.[22-24] In the last few years, the study of some amide-functionalized MOFs has confirmed their potential for selectively adsorb CO_2.[5, 22, 24-30] For example, Chen, Wang *et al.* have reported that pores decorated with acylamide groups in the Cu(II)-based UTSA-48 MOF promote strong interactions with CO_2 and high selectivity for CO_2 over CH_4.[5] Recently, Wang *et al.* reported a 3-fold interpenetrated acylamide-MOF that shows higher selective adsorption of CO_2 rather than other gases with a significant isosteric heat.[31] Similarly, Zaworotko *et al.* found that the decoration of a **rht**-type MOF also with acylamide functions can significantly enhance the CO_2 uptake and the selective adsorption of CO_2 over N_2 in comparison to PCN-61; an isoreticular analogue with acetylene moieties instead of amide groups.[24] Remarkably, comparable trends of selectivity have also been observed in other MOFs decorated with acylamide[25-28] and oxamide[22] groups as well as in some recent porous covalent organic frameworks also containing acylamide groups.[29, 30]

Recent studies reported by us have shown that a series of porous interpenetrated MOFs can be designed by pillaring 2D layers, comprising Zn(II) ions and the V-shaped dicarboxylate ligand 4,4′-oxybisbenzoic acid (H_2oba), with linear dipyridyl-based ligands (Fig. 1).[32-34] Following this approach, we found that the pores of the synthesized MOFs can be easily functionalized with the two groups incorporated in the pillar ligands since the pores of these MOFs, which run perpendicular to the {Zn(oba)} layers, are also delimited by these ligands.[29, 30, 35] For example, the use of the pillar ligands N,N′-bis-(4-pyridylmethylene)-1,4-benzenediamine (bpmb) and its naphthalene analogue N,N′-bis-(4-pyridylmethylene)-

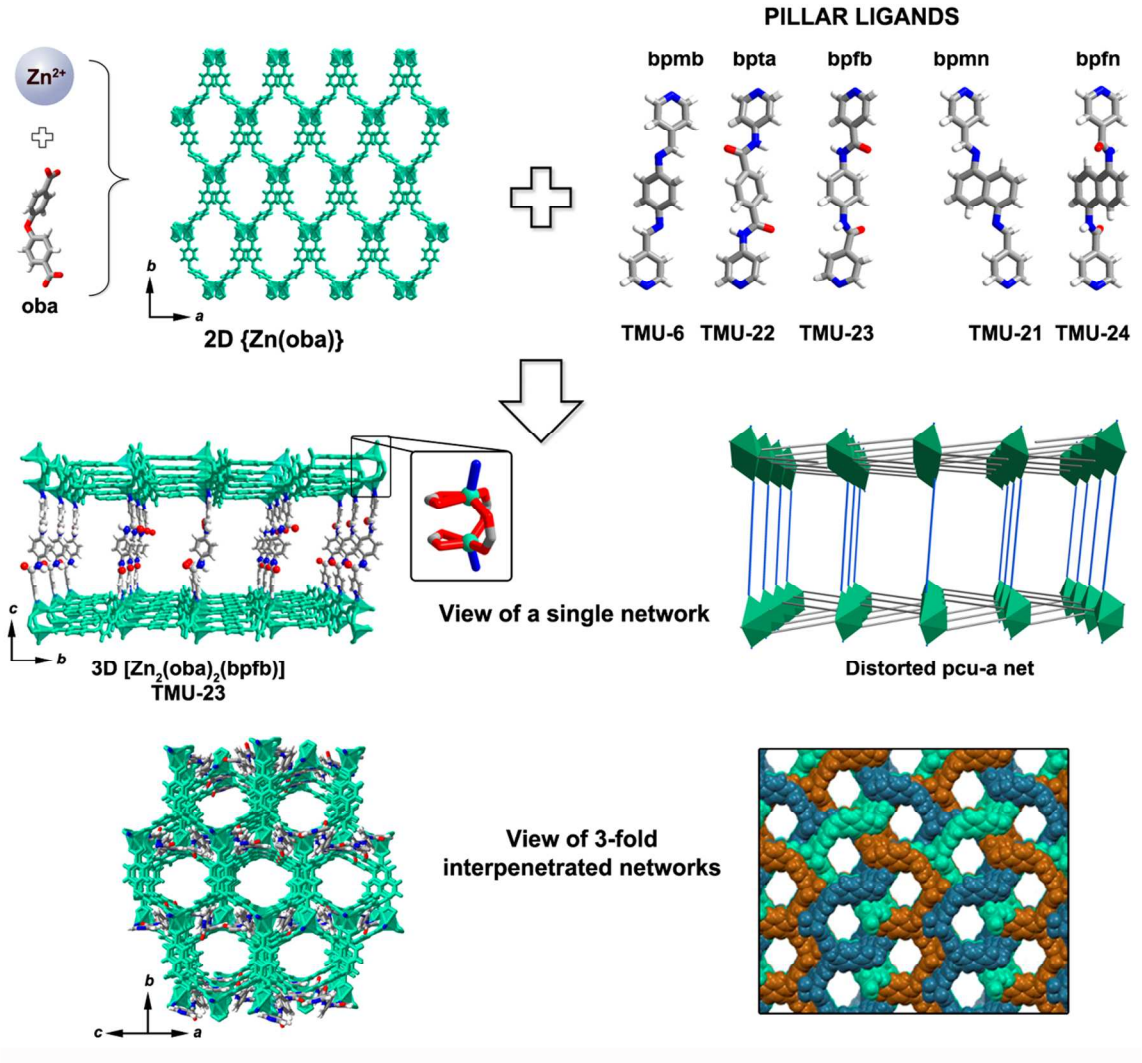

Figure 1. 2D layers formed by the association between Zn(II) ions and oba linkers are further pillared by amide/imine-functionalized dipyridyl-based ligands yielding to 3D-interpenetrated porous **pcu**-MOFs.

1,5-naphthalenediamine (bpmn) recently allowed the formation of two isoreticular 3-fold interpenetrated MOFs showing pores functionalized with imine groups [called **TMU-6** and **TMU-21** (TMU = Tarbiat Modares University)].[33, 34] Herein, inspired by this approach and the potential of the amide groups for enhancing the selectivity towards CO_2, we report the synthesis of three newly acylamide-containing MOFs. The selected pillar ligands are N,N′-bis(4-pyridinyl)-terephthalamide (bpta), N,N′-(1,4-phenylene)diisonicotinamide (bpfb), and N,N′-bis-(4-pyridylformamide)-1,5-naphthalenediamine (bpfn), Figures 1 and S1, which lead to the assembly of: $[Zn_2(oba)_2(bpta)]\cdot(DMF)_3$ (**TMU-22**; where DMF is N,N-dimethylformamide); $[Zn_2(oba)_2(bpfb)]\cdot(DMF)_5$ (**TMU-23**), in which the acylamide group is inverted in comparison to **TMU-22**; and $[Zn_2(oba)_2(bpfn)]\cdot(DMF)_2$ (**TMU-24**), in which the use of the naphthalene analogue also induces that the acylamide groups are more directed towards the pores than in **TMU-22** and **TMU-23** (Figure 2). Importantly, the resulting 3-fold interpenetrated **TMUs-22/-23/-24** are isoreticular to **TMU-6** and **TMU-21**. The similarities (structure and stability) and differences (functional group and accessibility) of these MOFs allow studying the influence of the amide and the imine groups on their N_2 and CO_2 sorption properties as well as on their selective sorption of CO_2 over N_2. More specifically, this latter selectivity was evaluated by performing kinetics and breakthrough experiments for a CO_2/N_2 gas mixture.

EXPERIMENTAL SECTION

Materials and Characterization

The commercially available reagents were used without further purification. Ligands, **TMU-6** and **TMU-21**, were synthesized following reported procedures.[33,34] See Supporting Information and Figure S1 for synthetic details. Elemental analyses were collected on a CHNS Thermo Scientific Flash 2000 elemental analyser. Powder X-ray diffraction (PXRD)

measurements were collected on a Philips X'pert diffractometer with monochromatic Cu-Kα radiation (λ_{Cu} = 1.5406 Å). Thermogravimetric analysis (TGA) were carried out in a Perkin Elmer Pyris 1 under N_2 atmosphere and heating rate of 10 °C/min. Fourier transform infra-red (FT-IR) spectra were recorded on a Bruker Tensor 27FTIR spectrometer equipped with a Golden Gate diamond attenuated total reflection (ATR) cell, in absorption mode at room temperature.

General synthesis of TMU-22, TMU-23 and TMU-24

A mixture of $Zn(NO_3)_2.6H_2O$ (0.297 g, 1 mmol), H_2oba (0.258 g, 1 mmol), and the corresponding amide ligand (0.5 mmol) and DMF (50 mL) was sonicated until all solids were uniformly dispersed (≈ 3 minutes) and divided into 7 glass vials. The vials were heated at 120 °C for 3 days and then cooled to room temperature. Colourless (**TMU-22**) and red-brown (**TMU-23** and **TMU-24**) crystals were obtained as pure phases, washed by DMF, and dried at room temperature.

Data for **TMU-22**. Yield: 44 %. FT-IR (cm^{-1}): 1691 (m), 1595 (vs), 1504 (s), 1395 (vs), 1331 (m), 1298 (m), 1238 (vs), 1160 (vs), 1098 (m), 777 (m), 659 (m), 524 (m). EA on solvent free sample: calcd. (%) for $C_{46}H_{30}N_4O_{12}Zn_2$: C, 57.46; H, 3.15; N, 5.83; found: C, 57.50; H, 3.11; N, 5.74.

Data for **TMU-23**. Yield: 36 %. FT-IR (cm^{-1}): 1673 (vs), 1597 (vs), 1540 (m), 1510 (m), 1399 (vs), 1309 (m), 1220 (vs), 1159 (s), 1088 (m), 1067 (m), 1014 (m), 801 (m), 658 (m), 524 (m). EA on solvent free sample: calcd. (%) for $C_{46}H_{30}N_4O_{12}Zn_2$: C, 57.46; H, 3.15; N, 5.83; found: C, 57.00; H, 3.10; N, 5.65.

Data for **TMU-24**. Yield: 38 %. IR (cm^{-1}): 1667 (vs), 1595 (vs), 1570 (m), 1505 (s), 1386 (vs), 1235(s), 1158 (vs), 1089 (m), 1065 (m), 1015 (m), 878 (m), 659 (m), 522 (m). EA on solvent free sample: calcd. (%) for $C_{50}H_{32}N_4O_{12}Zn_2$: C, 59.37; H, 3.19; N, 5.54; found: C, 57.10; H, 3.12; N, 5.01.

Crystallography

Crystallographic data for **TMU-22** and **TMU-23** were collected at 100 K at XALOC beamline at ALBA synchrotron[36] (λ = 0.79474 Å and 0.82653 Å, respectively). Data were indexed, integrated and scaled using the XDS[37] and IMOSFLM[38] programs. Absorption correction was not applied. SCXRD for **TMU-24** was collected at 293 K on a Bruker AXS SMART Apex diffractometer using graphite monochromated Mo-Kα radiation (λ = 0.71073 Å) and were corrected for Lorentz and polarization effects. The frames were integrated with the Bruker SAINT[39] software package. Absorption corrections were applied using the program SADABS[40] giving max./min. transmission factors of 1.000/0.270. The structures were solved by direct methods and subsequently refined by correction of F^2 against all reflections, using SHELXS2013[41] and SHELXL2013[42] within the WinGX package.[43] All non-hydrogen atoms were refined with anisotropic thermal parameters by full-matrix least-squares calculations on F^2 using the program SHELXL2013. Hydrogen atoms were inserted at calculated positions and constrained with isotropic thermal parameters. In **TMU-24**, the carbonyl group of the N,N-ligand is distorted in two positions with 55 % and 45 % of occupancy. The structures contain some disorder molecules. Attempts to adequately model of disordered DMF molecules (40 electrons) were unsatisfactory; therefore the PLATON/SQUEEZE[44] routine has been applied to mask out the disordered electron density. The residual electron density was assigned to 3, 5 and 1 molecules of DMF in **TMU-22** (509 electrons per unit cell), **TMU-23** (876 electrons located per unit cell) and in **TMU-24** (384 electrons per unit cell). Crystallographic and refinement data, and the main bond distances and angles are listed in Table 1 and Tables S1-3.

Table 1. Crystal and structure refinement data.

Compound	**TMU-22**	**TMU-23**	**TMU-24**
Emp. formula	$C_{55}H_{51}N_7O_{15}Zn_2$	$C_{61}H_{65}N_9O_{17}Zn_2$	$C_{28}H_{23}N_3O_7Zn$
Formula weight	1180.76	1326.96	578.86
Crystal system	Monoclinic	Monoclinic	Monoclinic
Space group	*P2₁/n*	*P2₁/c*	*C2/c*
CCDC ref.	1480227	1480228	1480229
Unit cell dimensions			
a (Å)	14.680(4)	15.110(3)	14.881(4)
b (Å)	24.780(5)	24.110(5)	24.993(6)
c (Å)	16.270(5)	15.910(5)	16.013(4)
β (deg)	113.27(5)	112.10(6)	111.422(5)
V ($Å^3$)	5437.0(2)	5370.2(2)	5544.0(2)
Z	4	4	8
F (000)	2440	2760	2384
θ range (°)	1.850-33.822	1.626-33.681	1.630-28.396
Ind. Refln. (R_{int})	11071 (0.1528)	12947 (0.1164)	6462 (0.0637)
Goodness-of-fit on F^2	1.331	1.090	1.018
Final R indices [I > 2σ(I)]	R1 = 0.1402 wR2 = 0.3805	R1 = 0.0939 wR2 = 0.2444	R1 = 0.0717 wR2 = 0.1819

Low-Pressure Sorption Measurements

Volumetric N_2 and CO_2 sorption isotherms were collected at 77 K (N_2) and 203 K, 258 K, 273 K, 288 K and 298 K (CO_2) using an ASAP 2020 HD (Micromeritics). Temperature was controlled by using a liquid nitrogen bath (77 K) or a Lauda Proline RP 890 chiller (203 K – 298 K). The total pore volumes (Vt) were calculated at P/P0 = 0.95 (N_2) and at 760 torr (CO_2).

Kinetics of adsorption

Kinetic evaluation of the sorbents was performed at 298 K in a home-made glass manometric adsorption equipment using pure gas components (CO_2 and N_2). This equipment is constituted by a manifold of a well-known volume (to define the initial gas dose), a sample holder containing the adsorbent and a pressure transducer. Prior to the adsorption experiment, the samples were degassed under vacuum at the activation temperature used for single gas sorption experiments. The initial pressure in the manifold was defined at 500 mbar for all adsorbates. Once equilibrated, the manifold was expanded to the sample holder, pressure readings being recorded every second and lasting for ten minutes. Moreover, the sample holder was immersed in a temperature-controlled water bath at 298 K to minimize any heat effect due to the adsorption process itself.

Breakthrough measurements

Breakthrough curve experiments for different mixture of gases were carried out using a column. The samples powders were packed in the middle part of the column. Here, the samples masses used were 0.30 g. The flow rates of all gases were controlled by mass flow controllers. Before the measurement, the samples were activated at the desired temperature for 2 h using a He total flow of 50 $mL.min^{-1}$.

The gas stream from the outlet of the column was analysed online with a mass spectrometer.

The CO_2/N_2 selectivities (σ) of samples were evaluated by the following equation:

$$\sigma = \frac{\left(\frac{q_{CO_2}}{p_{CO_2}}\right)}{\left(\frac{q_{N_2}}{p_{N_2}}\right)}$$

where q_i is the adsorption capacity of i component, p_i is the partial pressure of i component.

The amount adsorbed for each gas was calculated by the integration of the breakthrough curves. For this purpose, breakthrough experiments with H_2 (not adsorbed in these materials), have been performed using the same bed and the same flows. Then, the H_2 breakthrough curve has been used to calculate the time zero and more importantly to consider the shape of the breakthrough in the integration. The amount of gas adsorbed was the different between the shape of the CO_2 or N_2 breakthrough and the H_2 breakthrough. Thus, the dispersion and the very small pressure drop can be considered.

Results and discussion

Synthesis and crystal structures

TMUs-22/-23/-24 were synthesized following the same pillaring strategy reported for **TMU-6** and **TMU-21**.[33,34] Solvothermal reactions between $Zn(NO_3)_2.6H_2O$, H_2oba and the correspondent pillar ligand in DMF at 120 °C for 3 days produced prismatic crystals of **TMUs-22/-23/-24** suitable for single-crystal X-ray diffraction analyses. The simulated (derived from the single crystal structures) and experimental powder X-ray diffraction (PXRD) patterns were consistent (Figure S2), confirming that all synthesized MOFs can be obtained as pure phases; as also corroborated by Fourier transformed infrared spectroscopy and elemental analysis (performed on the activated samples, *vide infra*).

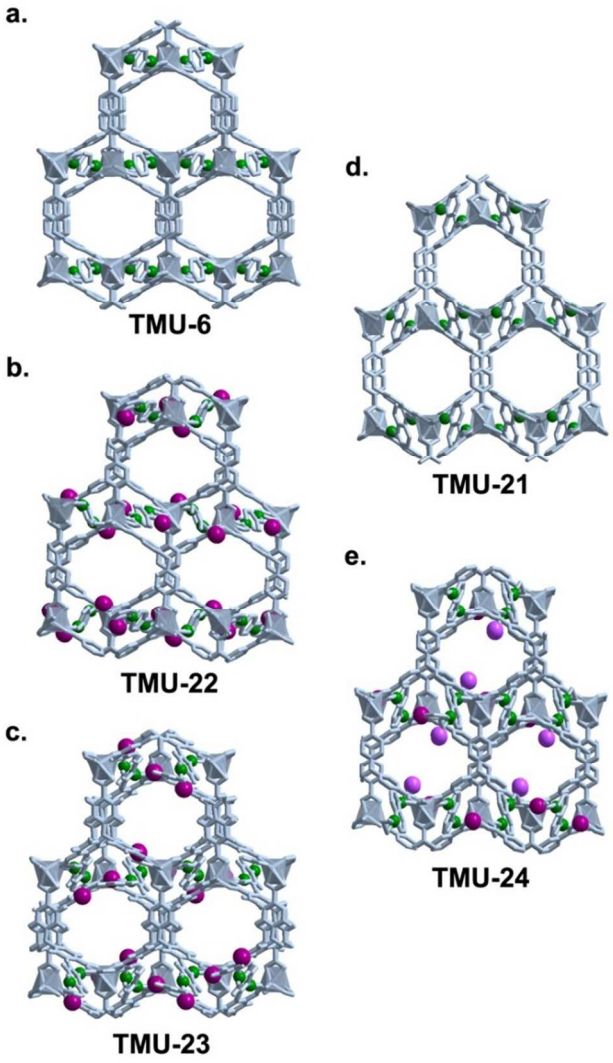

Figure 2. View of the pore channels of a) **TMU-6**, b) **TMU-22**, c) **TMU-23**, d) **TMU-21** and e) **TMU-24**, highlighting the acylamide groups. Colour code: N (green), O (purple), the more accessible O atoms in TMU-24 (lavender).

TMU-22 and **TMU-23** crystallize in the monoclinic $P2_1/n$ and $P2_1/c$ space groups, respectively (Table 1). They are neutral 3-fold interpenetrated MOFs formed by {Zn(oba)} layers connected through the N,N′-pillar ligands. As in **TMU-6**, their basic unit is a dinuclear zinc cluster, in which both Zn(II) centres are penta-coordinated to four carboxylate O atoms from three fully deprotonated oba ligands and to one N atom from the N,N′-donor ligand (Figure 1). The geometry around the metal centres can be described as a distorted square pyramid, with Addison parameter[45] τ values in the range of

0.35-0.49. In these structures, each nonlinear dicarboxylate oba ligand is coordinated to three Zn(II) centres forming the {Zn(oba)} layers along the ab plane. Because of the dinuclear nature of the metal cluster, these layers are formed by two sheets of parallel oba ligands that form π-π stacking interactions between them (Figure 1; Tables S4, S5). These {Zn(oba)} layers are then pillared by the linear acylamide-functionalized ligands, extending the structure in three dimensions. It is important to mention here that, due to the conformational flexibility of both oba and bpta ligands, **TMU-22** is a supramolecular conformational isomer of a reported MOF.[31] Although both compounds are 3-fold interpenetrated, they still possess apparent 1D pore channels (≈ 7.0 × 6.5 Å and ≈ 6.8 × 6.4 Å -including van der Waals (vdW) radii- for **TMU-22** and **TMU-23**, respectively) running along the <101> direction and noticeable free space (33 % for **TMU-22** and 32 % for **TMU-23**), comparable to the values found for **TMU-6** (≈ 8.1 × 7.4 Å; and 33 % free space)[46] (Figures 1 and S3-5). The channels are filled with disordered guest solvent molecules, squeezed due to thermal disorder.

TMU-24 crystallizes in the monoclinic *C2/c* space group (Table 1), showing a crystal structure isoreticular to those of **TMUs-6/-21/-22/-23**. Thus, it also consists on a 3-fold interpenetrated network that exhibits 1D pore channels of ≈ 6.7 × 5.5 Å (free space = 30 %) functionalized with acylamide groups. These values are similar to those exhibited by its imine-functionalized **TMU-21** analogue, which shows a pore size of ≈ 8.2 × 7.0 Å and a free space of 30 %.[46] (Figures S6-7).

Here it is very important to note that, even though **TMUs-22/-23/-24** are isoreticular, their acylamide groups do not show the same orientation on the pore surfaces (Figure 2b,c,e) as well as do not participate in the same number of supramolecular interactions between the interpenetrated networks (Tables S4-6). In **TMU-23**, all donor –N-H and acceptor –C=O groups of the two acylamide groups per pillar ligand establish H-bonds and N-H···π interactions with the other two networks forming the 3-fold interpenetrated structure. In **TMU-22**, each donor –NH moiety of the two acylamide groups per pillar ligand establishes H-bonds with carboxylate groups of the other networks, whereas the two acceptor -C=O groups do not participate in H-bonds. In **TMU-24**, only one of the two acylamide groups forms H-bonds. Interestingly, the other acylamide group is pointing towards the pores so that it does not participate in direct H-bonds with the other networks (Figure 2e). Altogether makes this acylamide group easily accessible to potential interactions with CO_2 guest molecules. Contrariwise, even though all the other H-bonded acylamide groups of **TMUs-22/-23/-24** are located on the surfaces of the pores, they are not directly pointing towards the channels, and therefore they are in principle less accessible to guest molecules.

Topology

Topological analysis performed with TOPOS[47] revealed that all the studied MOFs show the same 3-fold interpenetrated, 6-connected net with **pcu** topology (Figure 1). The **pcu** topology is ubiquitous in MOFs, including the iconic MOF-5.[48] Here, it is worth to mention that the **pcu** net is edge-transitive with cubic symmetry and *Pm-3m* space group. However, in the present case, the overall symmetry of **TMUs-22/-23/-24** decreased to monoclinic (Table 1). This symmetry decrease is attributed to the fact that the points of extension of the Zn(II) dimer do not match with the vertices of the perfect octahedron required to produce highly symmetrical **pcu**-MOFs (Figure 1). In addition, the use of a pillaring strategy with mixed ligands (including the flexible oba and pillar N,N′-ligands) also forces the symmetry to differ from that of MOF-5.

Thermal stability

The TGA diagrams of all as-synthesized materials revealed a first weight loss of 16.08 % (room temperature (r.t.)-300 °C) for **TMU-6**, 13.71 % (80-325 °C) for **TMU-21**, 9.93 % (100-240 °C) for **TMU-22**, 15.16 % (r.t.-300 °C) for **TMU-23**, and 15.46 % (r.t.-325 °C) for **TMU-24**. In all cases, this weight loss was attributed to the removal of all guest solvent molecules. Decomposition of all materials starts at around 400 ^{o}C, confirming their high thermal stability (Figure S8).

Activation process

All compounds were activated using a very similar protocol that started with a solvent-exchange step. **TMUs-6/-21** and **TMUs-22/-23/-24** were immersed in acetonitrile and dichloromethane, respectively, for 3 days, during which the solvent was exchanged once daily. Note here that previous stability tests showed that all synthesized MOFs were stable in these solvents (Figure S9) for at least 24 h at r.t. Then, each MOF was evacuated for 12 h under vacuum at 150 °C prior to gas sorption measurements. It is noteworthy that PXRD diagrams collected after the sorption studies confirm that the frameworks retain their crystallinity and remained unaltered after both processes (Figure S10). These observations were further corroborated by elemental analysis and TGA, in which only the weight loses around 400 ^{o}C corresponding to their decomposition were observed (Figure S8).

Nitrogen sorption at 77 K

N_2 isotherm at 77 K on **TMU-22** showed a characteristic type I behaviour of microporous materials, as expected from its crystal structure (BET area (A_{BET}) = 680 $m^2.g^{-1}$; pore volume (V_t) = 0.28 $cm^3.g^{-1}$). Contrariwise, **TMU-21**, **TMU-23** and **TMU-24** were found to be non-porous materials (negligible N_2 uptake). In the case of **TMU-6**, it showed much lower porosity than that expected from its crystal structure (A_{BET} = 150 $m^2.g^{-1}$; V_t = 0.08 $cm^3.g^{-1}$) (Table 2, Figure S11). Thus, all activated compounds, except **TMU-22**, reveal a "N_2-phobic" behavior.[49-52] We reasoned that this behaviour could be due to the existence of different structural rearrangements depending on the MOF during sorption or when exposed to cryogenic temperatures and/or under vacuum, reducing/preventing access to the porosity. Indeed, similar temperature dependent behaviours are already well-known in soft materials such as in MIL-53 (Al).[53] However, other factors cannot be fully excluded, such as the existence of strong interactions between N_2 and the channel walls at 77 K that hinder diffusion into the material.[54]

Table 2. Summary of BET areas, total pore volumes and CO_2 uptakes observed for TMUs-6/-21-24.

MOF	*A_{BET} ($m^2.g^{-1}$) (N_2, 77 K)*	*Total V_t ($cm^3.g^{-1}$) (N_2[a] / CO_2[b])*	*Theo V_t ($cm^3.g^{-1}$)[c]*	*CO_2 uptake[b] ($mmol.g^{-1}$) (203 K)*
TMU-6	150	0.08 / 0.32	0.22	9.0
TMU-21	≈ 0	≈ 0 / 0.16	0.25	4.5
TMU-22	680	0.28 / 0.25	0.25	7.2
TMU-23	≈ 0	≈ 0 / 0.27	0.27	7.2
TMU-24	≈ 0	≈ 0 / 0.22	0.25	6.3

[a] calculated at P/P_0 = 0.95. [b] Calculated at P = 760 torr. [c] Calculated with PLATON.

CO_2 sorption at various temperatures and heats of adsorption

Contrariwise to the adsorption of N_2, the CO_2 sorption isotherms at various temperatures revealed that all of them are porous (Figures 3a and S12a-16a). CO_2 uptake at 203 K were calculated to be 9.0 $mmol.g^{-1}$, 4.5 $mmol.g^{-1}$, 7.2 $mmol.g^{-1}$, 7.2 $mmol.g^{-1}$ and 6.3 $mmol.g^{-1}$ for **TMU-6**, **TMU-21**, **TMU-22**, **TMU-23** and **TMU-24**, respectively (Table 2). The observed pore volumes (at 760 torr) were: 0.32 $cm^3.g^{-1}$ (**TMU-6**), 0.16 $cm^3.g^{-1}$ (**TMU-21**), 0.25 $cm^3\ g^{-1}$ (**TMU-22**), 0.27 $cm^3.g^{-1}$ (**TMU-23**) and 0.22 $cm^3.g^{-1}$ (**TMU-24**). These pore volumes calculated from the CO_2 adsorption data are in agreement with the theoretical values extracted from the crystal structures. The variations observed can be attributed to small structural changes widely observed in such interpenetrated sorbents.[35, 55-57]

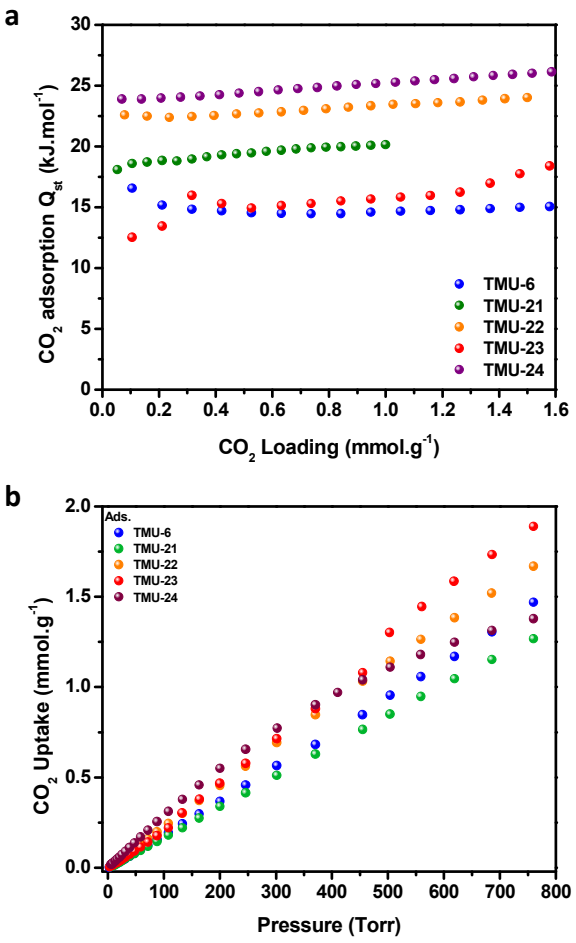

Figure 3. (a) Heats of adsorption of CO_2 and (b) CO_2 sorption isotherms at 298 K for **TMUs-6/-21-24**.

Isosteric heats of adsorption of CO_2 (Q_{st}) were calculated from the isotherms collected at different temperatures (Table 2 and Figures S12-16). The two acylamide-functionalized **TMU-24** and **TMU-22** exhibited the highest Q_{st} for CO_2, from 24 to 26 $kJ{\cdot}mol^{-1}$ and 23 to 24 $kJ{\cdot}mol^{-1}$, respectively. The different Q_{st} for CO_2 between **TMU-24**, **TMU-22**, and **TMU-23** can be attributable to the different accessibility of their acylamide groups and to the different number of supramolecular interactions in which they are involved (*vide supra*).

CO_2/N_2 separation properties

In light of the porosity of the materials for CO_2 and their apparent low affinity for N_2, we further investigated their potential for CO_2/N_2 separation by performing kinetics experiments (Figures 4 and S17). As expected, the highest selectivity (σ) for CO_2 over N_2 was observed for **TMU-24** (σ = 14.1, Table 3); which is the material exhibiting the highest Q_{st} of CO_2 and with the most accessible acylamide groups pointing towards the porous channels. Overall, the CO_2/N_2 selectivity of **TMU-24** estimated from kinetics experiment is *ca.* 70 % higher than for the other materials of the family.

These results were further confirmed by breakthrough experiments with CO_2/N_2 gas mixture (Figures 5 and S18). Once again, **TMU-24** performed much better than its isoreticular variants, with a CO_2/N_2 selectivity of 10.0 at r.t. for an equimolar CO_2/N_2 gas mixture (Figure 5). This value represents 700 % of the selectivity found in similar conditions for its imine analogue **TMU-21** (σ = 1.4). It also performs better than **TMU-22** and **TMU-23**, the other acylamide containing MOFs with less accessible functional groups. Indeed, the selectivity of **TMU-24** is 500 % and 580 % the selectivity of **TMU-22** and **TMU-23**, respectively. Therefore, not only the incorporation of amide functional groups in the frameworks but also their accessibility for the CO_2 guest molecules is crucial to enhance the CO_2/N_2 selectivity. This observation was further confirmed in more realistic gas mixture conditions (CO_2:N_2 = 1:9), in which **TMU-24** was still found to perform well with a selectivity of 4.6 (Figure 5). It is important to remark that the CO_2 adsorption capacity found in the breakthrough experiment at r.t. (≈ 0.65 mmol.g^{-1}) for **TMU-24** is slightly lower than the one extracted from the isotherm at 500 mbar and r.t. (≈ 0.85 mmol.g^{-1}). This feature can be attributed to a small amount of N_2 adsorbed in these conditions (298 K and gas mixture).

Table 3 Summary of CO_2 separation properties in TMUs-6/-21/-22/-23/-24.

MOF	Q_{st} of CO_2 (kJ.mol^{-1})	Selectivity (Kinetics)	Selectivity (Breakthrough, CO_2:N_2 1:1)
TMU-6	17-14	8.2	1.8
TMU-21	18-20	8.2	1.4
TMU-22	23-24	8.6	2.0
TMU-23	12-18	8.2	1.7
TMU-24	24-26	14.1	10.0

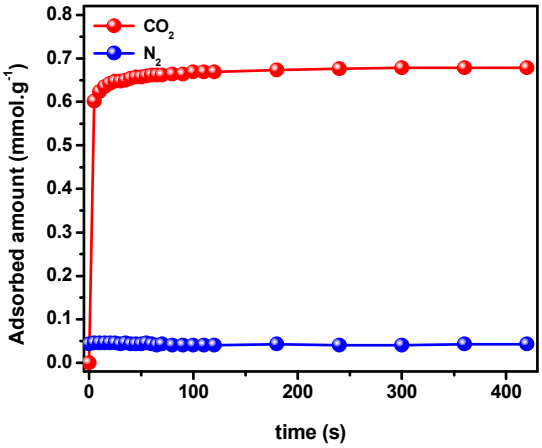

Figure 4. Adsorption kinetics of CO_2 and N_2 for **TMU-24** at 298 K (initial manifold pressure 500 mbar).

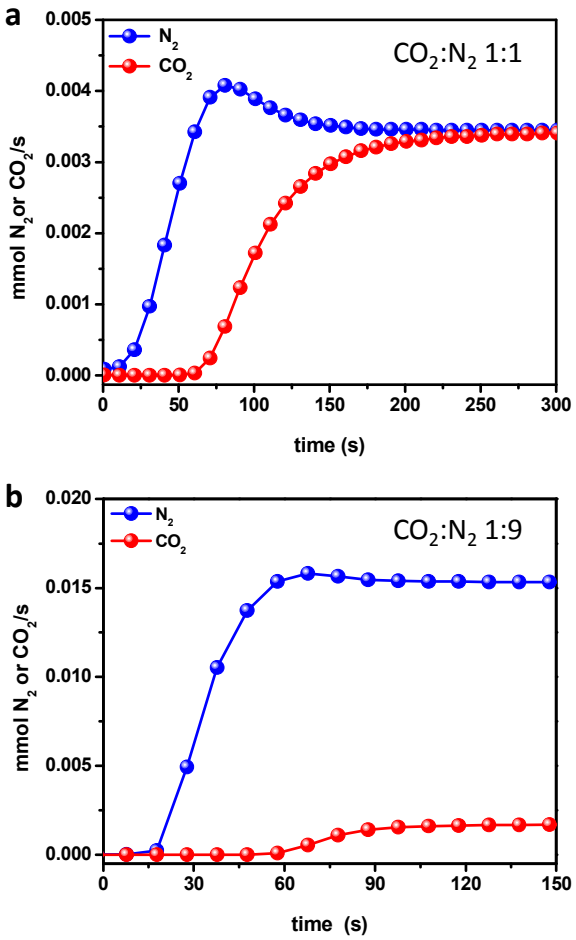

Figure 5. CO_2/N_2 Breakthrough separation curves at 298 K for **TMU-24** with total flow of 5 mL.min^{-1} for CO_2:N_2 = 1:1 (a) and 25 mL.min^{-1} for 1:9 (b).

CONCLUSIONS

We successfully synthesized three novel, 3-fold interpenetrated **pcu**-MOFs containing acylamide functional groups (**TMU-22**, **TMU-23** and **TMU-24**), isoreticular to the recently reported imine-containing MOFs, **TMU-6** and **TMU-21**. The study of their sorption properties revealed that the insertion of amide functional groups in MOFs does not necessarily induce a noticeable improvement of the CO_2/N_2 separation properties. Indeed, another aspect that needs to be addressed is the accessibility of the functional groups, especially in interpenetrated frameworks. If neglected, it could jeopardize the efficiency of MOFs functionalization, as illustrated by the performance of **TMU-22** and **TMU-23**, two acylamide-functionalized analogues of the parent imine-functionalized **TMU-6**; that all these three MOFs show negligible difference of the selectivity. This demonstrates the needs for smart materials design approaches, further confirmed by the deliberate alteration of the pore shape of **TMU-24** using a bulky, central naphthalene core. This resulted in better accessibility of the acylamide groups,

leading into a 70 % improvement of CO_2/N_2 selectivity according to kinetics studies (from 8.2 to 14.1 for **TMU-21** and **TMU-24**, respectively). Moreover, a dramatic increase of the selectivity was obtained from breakthrough experiments. The CO_2/N_2 selectivity for **TMU-24** corresponds to *ca.* 700 % of this imine- containing analogue, **TMU-21**. Moreover, its selectivity is *ca.* 500 % and 580 % of **TMU-22** and **TMU-23**, two isoreticular, amide containing MOFs with less accessible functional groups.

ASSOCIATED CONTENT

Supporting Information. Synthetic procedure for ligand synthesis, crystallographic data, PXRD diagrams, TGA plots, gas sorption and separation data. This material is available free of charge via the Internet at http://pubs.acs.org.

AUTHOR INFORMATION

Corresponding Authors

* E-mails: daniel.maspoch@icn2.cat, morsali_a@modares.ac.ir

Author Contributions

The manuscript was written through contributions of all authors. All authors have given approval to the final version of the manuscript.

Notes

The authors declare no competing financial interest.

ACKNOWLEDGMENTS

This work was supported by the MINECO-Spain through projects PN MAT2015-65354-C2-1-R, 2014-SGR-80, MAT2013-45008-P and EU FP7 ERC-Co 615954. I.I. and E.V.R.F. thank the MINECO for the RyC fellowship RYC-2010-06530 and RyC-2012-11427 and V.G. is grateful to the Generalitat de Catalunya for a Beatriu de Pinós Fellowship. ICN2 acknowledges the support of the Spanish MINECO through the Severo Ochoa Centers of Excellence Program, under Grant SEV-2013-0295. E.V.R.F. and J.S.A. acknowledge the Generalitat Valenciana for PROMETEOII/2014/004. Support of this investigation by Tarbiat Modares University is gratefully acknowledged.

REFERENCES

(1) Zhou, H. C.; Long, J. R.; Yaghi (Eds.), O. M., Themed issue: Metal-Organic Frameworks, *Chem. Rev.*, **2012**, *112*, 673-1268
(2) Long, J. R.; Yaghi (Eds.), O. M., Themed issue: Metal-Organic Frameworks, *Chem. Soc. Rev.*, **2009**, *38*, 1201-1508
(3) Zhou, H. C.; Kitagawa (Eds.), S., Themed issue: Metal-Organic Frameworks, *Chem. Soc. Rev.*, **2014**, *43*, 5415-6172
(4) Belmabkhout, Y.; Guillerm, V.; Eddaoudi, M., *Chem. Eng. J.* **2016,** *296*, 386-397.
(5) Xiong, S.; He, Y.; Krishna, R.; Chen, B.; Wang, Z., *Cryst. Growth Des.* **2013,** *13*, 2670-2674.
(6) Sumida, K.; Rogow, D. L.; Mason, J. A.; McDonald, T. M.; Bloch, E. D.; Herm, Z. R.; Bae, T.-H.; Long, J. R., *Chem. Rev.* **2012,** *112*, 724-781.
(7) Liu, J.; Thallapally, P. K.; McGrail, B. P.; Brown, D. R.; Liu, J., *Chem. Soc. Rev.* **2012,** *41*, 2308-2322.
(8) Vaidhyanathan, R.; Iremonger, S. S.; Shimizu, G. K.; Boyd, P. G.; Alavi, S.; Woo, T. K., *Science* **2010,** *330*, 650-653.
(9) Li, B.; Zhang, Z.; Li, Y.; Yao, K.; Zhu, Y.; Deng, Z.; Yang, F.; Zhou, X.; Li, G.; Wu, H., *Angew. Chem. Int. Ed.* **2012,** *51*, 1412-1415.
(10) Panda, T.; Pachfule, P.; Banerjee, R., *Chem. Commun.* **2011,** *47*, 7674-7676.
(11) Caskey, S. R.; Wong-Foy, A. G.; Matzger, A. J., *J. Am. Chem. Soc.* **2008,** *130*, 10870-10871.
(12) Zhang, S.-Y.; Zhang, X.; Li, H.; Niu, Z.; Shi, W.; Cheng, P., *Inorg. Chem.* **2015,** *54*, 2310-2314.
(13) Llewellyn, P. L.; Bourrelly, S.; Serre, C.; Vimont, A.; Daturi, M.; Hamon, L.; De Weireld, G.; Chang, J.-S.; Hong, D.-Y.; Kyu Hwang, Y.; Hwa Jhung, S.; Férey, G., *Langmuir* **2008,** *24*, 7245-7250.
(14) Chen, D.-M.; Xu, N.; Qiu, X.-H.; Cheng, P., *Cryst. Growth Des.* **2015,** *15*, 961-965.
(15) McDonald, T. M.; Mason, J. A.; Kong, X.; Bloch, E. D.; Gygi, D.; Dani, A.; Crocella, V.; Giordanino, F.; Odoh, S. O.; Drisdell, W. S.; Vlaisavljevich, B.; Dzubak, A. L.; Poloni, R.; Schnell, S. K.; Planas, N.; Lee, K.; Pascal, T.; Wan, L. F.; Prendergast, D.; Neaton, J. B.; Smit, B.; Kortright, J. B.; Gagliardi, L.; Bordiga, S.; Reimer, J. A.; Long, J. R., *Nature* **2015,** *519*, 303-308.
(16) Couck, S.; Denayer, J. F.; Baron, G. V.; Rémy, T.; Gascon, J.; Kapteijn, F., *J. Am. Chem. Soc.* **2009,** *131*, 6326-6327.
(17) Demessence, A.; D'Alessandro, D. M.; Foo, M. L.; Long, J. R., *J. Am. Chem. Soc.* **2009,** *131*, 8784-8785.
(18) Fracaroli, A. M.; Furukawa, H.; Suzuki, M.; Dodd, M.; Okajima, S.; Gándara, F.; Reimer, J. A.; Yaghi, O. M., *J. Am. Chem. Soc.* **2014,** *136*, 8863-8866.
(19) Nugent, P.; Belmabkhout, Y.; Burd, S. D.; Cairns, A. J.; Luebke, R.; Forrest, K.; Pham, T.; Ma, S.; Space, B.; Wojtas, L.; Eddaoudi, M.; Zaworotko, M. J., *Nature* **2013,** *495*, 80-84.
(20) Shekhah, O.; Belmabkhout, Y.; Chen, Z.; Guillerm, V.; Cairns, A.; Adil, K.; Eddaoudi, M., *Nature Commun.* **2014,** *5*, 4228.
(21) de Lange, K. M.; Lane, J. R., *J. Chem. Phys.* **2011,** *135*, 064304.
(22) Alsmail, N. H.; Suyetin, M.; Yan, Y.; Cabot, R.; Krap, C. P.; Lü, J.; Easun, T. L.; Bichoutskaia, E.; Lewis, W.; Blake, A. J.; Schröder, M., *Chem. Eur. J.* **2014,** *20*, 7317-7324.
(23) Bent, H. A., *Chem. Rev.* **1968,** *68*, 587-648.
(24) Zheng, B.; Bai, J.; Duan, J.; Wojtas, L.; Zaworotko, M. J., *J. Am. Chem. Soc.* **2011,** *133*, 748-751.
(25) Lu, Z.; Xing, H.; Sun, R.; Bai, J.; Zheng, B.; Li, Y., *Cryst. Growth Des.* **2012,** *12*, 1081-1084.
(26) Zheng, B.; Liu, H.; Wang, Z.; Yu, X.; Yi, P.; Bai, J., *CrystEngComm* **2013,** *15*, 3517-3520.
(27) Duan, J.; Yang, Z.; Bai, J.; Zheng, B.; Li, Y.; Li, S., *Chem. Commun.* **2012,** *48*, 3058-3060.
(28) Park, J.; Li, J.-R.; Chen, Y.-P.; Yu, J.; Yakovenko, A. A.; Wang, Z. U.; Sun, L.-B.; Balbuena, P. B.; Zhou, H.-C., *Chem. Commun.* **2012,** *48*, 9995-9997.
(29) Luo, X.-Z.; Jia, X.-J.; Deng, J.-H.; Zhong, J.-L.; Liu, H.-J.; Wang, K.-J.; Zhong, D.-C., *J. Am. Chem. Soc.* **2013,** *135*, 11684-11687.
(30) Rajput, L.; Banerjee, R., *Cryst. Growth Des.* **2014,** *14*, 2729-2732.
(31) Lin, R.-G.; Cao, G.-J.; Lin, J.-D.; Wang, Y.-L., *New J. Chem.* **2015,** *39*, 9075-9078.
(32) Guillerm, V.; Kim, D.; Eubank, J. F.; Luebke, R.; Liu, X.; Adil, K.; Lah, M. S.; Eddaoudi, M., *Chem. Soc. Rev.* **2014,** *43*, 6141-6172.
(33) Masoomi, M. Y.; Beheshti, S.; Morsali, A., *J. Mater. Chem. A* **2014,** *2*, 16863-16866.
(34) Azhdari Tehrani, A.; Ghasempour, H.; Morsali, A.; Makhloufi, G.; Janiak, C., *Cryst. Growth Des.* **2015,** *15*, 5543-5547.

(35) Masoomi, M. Y.; Stylianou, K. C.; Morsali, A.; Retailleau, P.; Maspoch, D., *Cryst. Growth Des.* **2014,** *14*, 2092-2096.
(36) Juanhuix, J.; Gil-Ortiz, F.; Cuni, G.; Colldelram, C.; Nicolas, J.; Lidon, J.; Boter, E.; Ruget, C.; Ferrer, S.; Benach, J., *J. Synchr. Rad.* **2014,** *21*, 679-689.
(37) Kabsch, W., *Acta Cryst. Sect. D* **2010,** *66*, 125-132.
(38) Leslie, A., *Acta Cryst. Sect. D* **2006,** *62*, 48-57.
(39) *Siemens SAINT, 4*. Siemens Analytical X-ray Instruments Inc.: Madison, Wisconsin, USA., 1996.
(40) Krause, L.; Herbst-Irmer, R.; Sheldrick, G. M.; Stalke, D., *J. Appl. Crystallogr.* **2015,** *48*, 3-10.
(41) Sheldrick, G. M.; Dauter, Z.; Wilson, K. S.; Hope, H.; Sieker, L. C., *Acta Cryst. Sect. D* **1993,** *49*, 18-23.
(42) Sheldrick, G., *Acta Cryst. Sect. C* **2015,** *71*, 3-8.
(43) Farrugia, L., *J. Appl. Crystallogr.* **2012,** *45*, 849-854.
(44) Spek, A. L., *PLATON A Multipurpose Crystallographic Tool*. Utrecht University: Utrecht (The Netherlands), 2001.
(45) Addison, A. W.; Rao, T. N.; Reedijk, J.; van Rijn, J.; Verschoor, G. C., *J. Chem. Soc., Dalton Trans.* **1984**, 1349-1356.
(46) Spek, A. L., *J. Appl. Crystallogr.* **2003,** *36*, 7-13.
(47) Blatov, V. A.; Shevchenko, A. P.; Proserpio, D. M., *Cryst. Growth Des.* **2014,** *14*, 3576-3586.
(48) Li, H.; Eddaoudi, M.; O'Keeffe, M.; Yaghi, O. M., *Nature* **1999,** *402*, 276-279.
(49) Patel, H. A.; Hyun Je, S.; Park, J.; Chen, D. P.; Jung, Y.; Yavuz, C. T.; Coskun, A., *Nature Commun.* **2013,** *4*, 1357.
(50) Ok, K. M.; Sung, J.; Hu, G.; Jacobs, R. M. J.; O'Hare, D., *J. Am. Chem. Soc.* **2008,** *130*, 3762-3763.
(51) Jiang, J.-J.; Pan, M.; Liu, J.-M.; Wang, W.; Su, C.-Y., *Inorg. Chem.* **2010,** *49*, 10166-10173.
(52) Maji, T. K.; Matsuda, R.; Kitagawa, S., *Nat Mater* **2007,** *6*, 142-148.
(53) Liu, Y.; Her, J.-H.; Dailly, A.; Ramirez-Cuesta, A. J.; Neumann, D. A.; Brown, C. M., *J. Am. Chem. Soc.* **2008,** *130*, 11813-11818.
(54) Thomas-Gipson, J.; Beobide, G.; Castillo, O.; Cepeda, J.; Luque, A.; Perez-Yanez, S.; Aguayo, A. T.; Roman, P., *CrystEngComm* **2011,** *13*, 3301-3305.
(55) Horike, S.; Shimomura, S.; Kitagawa, S., *Nature Chem.* **2009,** *1*, 695-704.
(56) Schneemann, A.; Bon, V.; Schwedler, I.; Senkovska, I.; Kaskel, S.; Fischer, R. A., *Chem. Soc. Rev.* **2014,** *43*, 6062-6096.
(57) Férey, G.; Serre, C., *Chem. Soc. Rev.* **2009,** *38*, 1380-1399.

For Table of Contents Use Only

The influence of the amide groups in the CO_2/N_2 selectivity of a series of isoreticular, interpenetrated metal-organic frameworks.

Vahid Safarifard, Sabina Rodríguez-Hermida, Vincent Guillerm, Inhar Imaz, Mina Bigdeli, Alireza A. Tehrani, Jordi Juanhuix, Ali Morsali,* Mirian E. Casco, Joaquín Silvestre-Albero, Enrique V. Ramos-Fernandez and Daniel Maspoch*

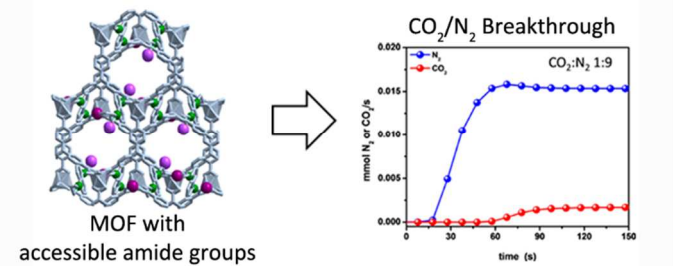

The accessibility of amide functional groups within MOF structures is crucial to obtain enhanced CO_2 sorption and CO_2/N_2 selectivity.